# Development and Demonstration of an Artificial Immune Algorithm for Mangrove Mapping Using Landsat TM

Yanmin Luo, Minghong Liao, Jing Yan, Caiyun Zhang, and Shaoling Shang

***Abstract*—Mangroves are valuable contributors to coastal ecosystems; knowledge of the dynamics of mangrove ecosystems is important in the context of global change. To obtain this knowledge, remote sensing is an indispensable means, yet it poses challenges since the accuracy is sometimes unsatisfactory in distinguishing mangroves from other land cover types with traditional classification methods. In this letter, we proposed a modified artificial immune algorithm (AIA), in which the antibodies represent the candidate solutions and the antigens are expressed by the fitness function. Multiclass coevolution was combined with the concept of clonal selection to ensure computation of an optimal clustering center in parallel for each land cover type. A cluster-center-oriented decimal encoding method for antibodies was adopted, and the inner class variance and the between-class difference together were used to formulate the fitness function. Furthermore, a design of the antibody solubility-based selection operator and nonuniform mutation operator was undertaken. Applying this modified AIA to a Landsat Thematic Mapper multispectral remote sensing imagery in the Zhangjiang estuary in southeastern China, we found that the AIA substantially improved classification accuracy over traditional methods, showing an overall accuracy of 90% (kappa coefficient = 0.88) and was capable to discern mangrove well (commission of 10% and omission of 22%).**

***Index Terms*—Artificial immune, classification, clonal selection, mangrove, remote sensing.**

## I. Introduction

MANGROVES are an important component of the world's coastal ecosystems [1]. Remote sensing technology provides a new way to detect and analyze the distribution of mangroves, which provides information needed for their protection. A core issue in mangrove remote sensing is image classification [2]–[4]. Since there are similar spectral features in mangroves and other land cover types, the phenomena of "same object with different spectra" and "same spectrum foreign matter" are widespread in spectral images; as a result, misclassification and leakage points are common, leading to low classification accuracy [5]. This makes it necessary to develop new ways to improve the classification accuracy of mangroves. Many efforts have been paid to the development of new techniques such as support vector machine (SVM) and object-based image analysis approach, yielding high accuracy for classifying mangroves [6]–[8].

The artificial immune algorithm (AIA) is a new machine-learning technique, which is inspired by human immune system and offers similar features to biological immune systems, such as noise tolerance, unsupervised learning, self-organization, and memory mechanism. A higher search success probability and improved individual diversity is thus achieved, enabling the AIA to well resolve problems in nonlinear classifications. There are various types of AIA, one of which is the clonal selection algorithm. It is derived from the clonal selection principle, which simulates B cells that protect the human body against attacks from antigens and eliminate infected cells [9]. Successful application of the clonal selection algorithm to various engineering problems has been demonstrated [10]–[13]. However, this algorithm has not been explicitly applied to satellite data processing in an attempt to discriminate mangrove vegetation from neighboring ecosystems.

This letter proposes a clonal selection-based AIA for mangrove detection from satellite images. In this approach, multiclass coevolution is combined with clonal selection to determine the best cluster centers for various land cover types in parallel. Furthermore, a cluster-center-oriented decimal encoding method for the antibodies is used which is suitable for remote sensing data. The inner class variance and the between-class difference are used together to measure the superiority of the antibodies, while the antibodies' solubility-based selection operator and nonuniform mutation operator are designed to guarantee diversity and global optimality. Finally, an experiment is performed on a Landsat Thematic Mapper (TM) multispectral remote sensing imagery in the Zhangjiang estuary in southeastern China. The results show that the proposed method can effectively improve the accuracy of mangrove extraction.

Manuscript received March 23, 2012; revised July 31, 2012 and September 16, 2012; accepted September 21, 2012. This work was supported in part by the National Basic Research Program of China under Contract 2009CB426306, by the National Science Foundation (NSF) of China under Contract 40976068, by the NSF of Fujian under Contract 2012J01273, and by Quanzhou scientific and technological planning project under Contract 2010Z53. *(Corresponding author: S. Shang.)*

Y. Luo is with the College of Computer Science and Technology, Huaqiao University, Xiamen 361021, China, and also with the Department of Cognitive Science, and Fujian Key Laboratory of the Brain-Like Intelligent Systems, Xiamen University, Xiamen 361005, China.

M. Liao is with the Software School, Xiamen University, Xiamen 361005, China (e-mail: liao@xmu.edu.cn).

J. Yan and C. Zhang are with the State Key Laboratory of Marine Environmental Science, Xiamen University, Xiamen 361005, China.

S. Shang is with the Key Laboratory of Underwater Acoustic Communication and Marine Information Technology (Xiamen University), Ministry of Education of China, Xiamen 361005, China (e-mail: slshang@xmu.edu.cn).

Color versions of one or more of the figures in this paper are available online at http://ieeexplore.ieee.org.

Digital Object Identifier 10.1109/LGRS.2012.2221675

## II. Immune Algorithm for Learning the Cluster Center

In the proposed AIA, the antibodies represent the candidate solutions, and the antigens are expressed by the fitness function. The coding way of the antibodies and the design of the fitness function are critical to the implementation of the algorithm.

Let $N_f$ be the number of the features in each training sample. Thus, each sample is an $N_f$-dimensional feature vector, given that there are $N_c$ different land cover types in a remote sensing image. The same number of training samples is extracted for each land cover type. Let $N_t$ be the number of training samples per type, so that the total number of the training samples is $N = N_t \times N_c$. Let $X = \{X^{(1)}, X^{(2)}, \ldots, X^{(N_c)}\}$ be the training sample set, where $X^{(i)} = \{X_1^{(i)}, X_2^{(i)}, \ldots, X_{N_t}^{(i)}\}$ is a subset of $X$ that consists of the samples for the $i$th land cover type. $X_j^{(i)} = (X_{j,1}^{(i)}, X_{j,2}^{(i)}, \ldots, X_{j,N_f}^{(i)})$ represents the $N_f$-dimensional feature vector of the $j$th sample in the $i$th class training sample set.

### A. Coding of the Antibodies

In AIAs, a binary format is most commonly used to code the antibodies and antigens due to its simplicity and convenient operations. However, for remote sensing data, the number of samples is generally far greater than the number of categories, and generally, the sample features are real numbers. Therefore, binary coding is not suitable for remote sensing data. Instead, we propose a cluster-center-based real encoding method, which is straightforward, effective, and suitable for parallel evolution and avoids the repetitious operation of encoding and decoding the binary code.

The antibodies (Ab) are composed of the $N_c$ clustering centers, $\text{Ab} = (C_1, C_2, \ldots, C_{N_c})$, where $C_i$ $(i = 1, 2, \ldots, N_c)$ is the cluster center of the $i$th land cover type. The $C_i$ of the initial antibody is generated by taking a sample randomly from the training sample set of the $i$th land cover type, $C_i = X_j^{(i)} = (x_{j,1}^{(i)}, x_{j,2}^{(i)}, \ldots, x_{j,N_f}^{(i)})$, where $j$ is a random number, $j \in [1, N_t]$.

As the immune algorithm evolves, it achieves optimal cluster centers for all land cover types that well represent their respective training samples. The antibodies in the memory set will converge to the optimal cluster centers step by step with the evolution process.

### B. Affinity Measure

The evolutionary search in the immune algorithm is based on an affinity function which measures the superiority of the antibodies. The affinity function determines the convergence speed of the evolution and affects the search of the optimal solution. Here, an affinity function was designed to determine the optimal cluster center for each land cover type by coevolution. The optimal cluster center should satisfy the two conditions provided as follows.

First, each cluster center can effectively represent its training samples, which means that it achieves the minimum inner class variances.

Second, the difference between any two classes should be as great as possible, which means that it achieves the maximum between-class differences.

In detail, for an antibody $\text{Ab} = (C_1, C_2, \ldots C_{N_c})$, in order to detect whether $C_i = (c_{i,1}, c_{i,2}, \ldots, c_{i,N_f})$ is suitable as the cluster center of its class, we defined the superiority of $C_i$, i.e., $\sup(C_i)$, as the variance of $C_i$ within the $i$th type as follows:

$$\begin{aligned}\sup(C_i) &= \frac{1}{N_t}\sum_{j=1}^{N_t}\sqrt{\left\|X_j^{(i)} - C_i\right\|^2} \\ &= \frac{1}{N_t}\sum_{j=1}^{N_t}\sum_{k=1}^{N_f}\sqrt{\left(x_{j,k}^{(i)} - c_{i,k}\right)^2} \end{aligned} \tag{1}$$

where $\|\cdots\|$ is Euclidean distance. By the nature of the variance, the superior $C_i$ has a smaller value of $\sup(C_i)$. Since Ab is composed of the cluster centers of all the classes, its inner class variance Sup(Ab) is defined as the sum of the variances of all the classes

$$\begin{aligned}\text{Sup(Ab)} &= \sum_{i=1}^{N_c}\sup(C_i) = \sum_{i=1}^{N_c}\left(\frac{1}{N_t}\sum_{j=1}^{N_t}\sqrt{\left\|X_j^{(i)} - C_i\right\|^2}\right) \\ &= \sum_{i=1}^{N_c}\left(\frac{1}{N_t}\sum_{j=1}^{N_t}\sum_{k=1}^{N_f}\sqrt{\left(x_{j,k}^{(i)} - c_{i,k}\right)^2}\right). \end{aligned} \tag{2}$$

A superior antibody has a smaller value of Sup(Ab).

The difference between any two cluster centers $C_i$ and $C_j$, i.e., $d(C_i, C_j)$, is calculated by

$$d(C_i, C_j) = \|C_i - C_j\| = \sqrt{\sum_{k=1}^{N_f}(c_{i,k} - c_{j,k})^2} \tag{3}$$

where $\|C_i - C_j\|$ is the Euclidean distance between $C_i$ and $C_j$. The between-class differences of an antibody Diff(Ab) are defined as the sum of the differences between any two cluster centers in the antibody Ab

$$\text{Diff(Ab)} = \sum_{i=1}^{N_c}\sum_{j=i+1}^{N_c} d(C_i, C_j). \tag{4}$$

A superior antibody has a larger value of Diff(Ab).

The affinity function of the immune algorithm fit(Ab) is given as follows:

$$\text{fit(Ab)} = \frac{\text{Diff(Ab)}}{\text{Sup(Ab)}}. \tag{5}$$

The value of the fit(Ab) represents the antigen–antibody (Ag−Ab) affinity. An excellent antibody has higher values of the affinity function and is more favorable for the classification.

### C. Immune Operators

The immune operators enable the new antibodies to match the antigen more closely, and they directly affect the convergence speed of the immune algorithm. Here, two

immune operators are involved in the evolution of the antibodies: clone selection and mutation. These are the same as those responsible for the evolution of species reproduction in a biological immune system.

*Antibody Solubility-Based Clone Selection Operator:* We adopted an antibody solubility-based clone selection operator. This operator not only ensures the diversity of antibodies but also makes the antibodies with high solubility have better chances to persist to the next generation. Let an antibody set be $S = \{\mathrm{Ab}_1, \mathrm{Ab}_2, \ldots, \mathrm{Ab}_{N_a}\}$, where $N_a$ is the number of antibodies in the set; the solubility of the antibody $\mathrm{Ab}_i$, i.e., density $(\mathrm{Ab}_i)$, can be computed by

$$\text{density}\ (\mathrm{Ab}_i) = \frac{1}{\sum_{j=1}^{N_a} \|\mathrm{Ab}_i - \mathrm{Ab}_j\|} \tag{6}$$

where $\|\mathrm{Ab}_i - \mathrm{Ab}_j\|$ is the Euclidean distance between $\mathrm{Ab}_i$ and $\mathrm{Ab}_j$. Based on the notion that an antibody with high solubility is closer to the cluster centers and should have a better opportunity to be cloned, the selection rate of an antibody is proportional to the solubility of the antibody. Therefore, the antibody solubility-based selection probability of antibody $\mathrm{Ab}_i$, i.e., $P_{\mathrm{clone}}(\mathrm{Ab}_i)$, can be computed by

$$P_{\mathrm{clone}}(\mathrm{Ab}_i) = \frac{\text{density}\ (\mathrm{Ab}_i)}{\sum_{j=1}^{N_a} \text{density}\ (\mathrm{Ab}_j)}. \tag{7}$$

Then, the selected antibodies are submitted, generating $N_{\mathrm{select}}$ antibodies to be cloned. The clone operation is subsequently performed. The clone size of a selected antibody $(N_{\mathrm{clone}})$ is an increasing function of antibody affinity, shown as follows:

$$N_{\mathrm{clone}}(i) = \text{round}\left(\frac{\beta \times N}{i}\right) \tag{8}$$

where $i$ is the affinity order of the cloned antibodies, $\beta$ is the multiplying factor of the clone operator, $N$ is the total number of antibodies, and round() is the operator that rounds its argument toward the closest integer. The solubility-based clone selection ensures that the antibodies evolve toward the cluster centers.

*Nonuniform Hypermutation Operator:* A nonuniform hypermutation operator based on a predefined mutation probability ($P_m$; see the number in Section II-D) was applied to perform mutation on selected cloned antibodies. The operator is compatible with decimal encoding and produces a new antibody by adding a random number to a given antibody.

Suppose that the mutation element is $C_k$ $(k = 1, 2, \ldots, N_c)$ for a given antibody $\mathrm{Ab} = (C_1, C_2, \ldots, C_{N_c})$, the offspring antibody generated by nonuniform hypermutation is $\mathrm{Ab}' = (C_1, C_2, \ldots, C'_k, \ldots, C_{N_c})$. $C'_k$ is built in the following way.

First, several features from $C_k = (c_{k,1}, c_{k,2}, \ldots, c_{k,N_f})$ are selected randomly. Second, the selected feature $c_{k,i}$ $(i = 1, 2, \ldots, N_f)$ undergoes mutation by randomly choosing either (9) or (10) to obtain the new antibody

$$c'_{k,i} = c_{k,i} + \Delta\left(t, c^U_{k,i} - c_{k,i}\right) \tag{9}$$

$$c'_{k,i} = c_{k,i} - \Delta\left(t, c_{k,i} - c^L_{k,i}\right). \tag{10}$$

**BEGIN**

1. Generate the initial antibody population ($P_{ini}$) and memory cells ($M$);

**REPEAT**

2. Use antibody solubility-based selection operator to select the individuals with high solubility from the population ($P_{ini}$);
3. Clone these individuals to form a temporary population of clones ($T$). The clone size is an increasing function of the antibody affinity;
4. Perform the non-uniform hyper-mutation on the population of clones ($T$), and generate the maturated antibody population ($T^*$);
5. Update the memory cells ($M$) by selecting superior antibodies from ($T^*$);
6. Replace the antibodies with the lowest affinity in ($P_{ini}$) with superior ones; the lower affinity, the higher probabilities to be replaced;

**UNTIL** a termination criterion is satisfied or predetermined generation number is reached;

**END**

Fig. 1. Description of the AIA.

Here, $c^U_{k,i}$ and $c^L_{k,i}$ are the upper and lower bounds of $c_{k,i}$, respectively, and $t$ is the iteration number. The function $\Delta(t, y) = y \cdot (1 - r^{(1-(t/M))^b})$ generates a random number which approaches zero with the increase of $t$, where $r$ is a random number ranging between zero and one, $M$ is the maximum iteration number, and $b \in [0, 1]$ is a parameter that determines the degree of nonconformance.

### D. Classification

Based on the coding way of the antibodies and the design of the fitness function as described earlier, we developed an AIA suitable for classifying mangroves (Fig. 1). The algorithm executes the loop from step 2 to step 6. After each loop, one generation of antibody is generated. The loop will terminate when a criterion is satisfied or a predetermined generation number is reached. The cluster centers of the various land cover types are then determined.

Subsequently, the minimum distance method is used to classify the remote sensing images. The distance function used here is Mahalanobis distance [14], where the covariance matrix of the $i$th land cover type is built by selecting the best members from memory set $M$.

Finally, the implementation of the algorithm requires proper setting of the number of selected antibodies to be cloned $(N_{\mathrm{select}})$, the multiplying factor of the clone operator $(\beta)$, and the mutation probability $(P_m)$. It is found that, when $N_{\mathrm{select}}$ was set as five, $\beta$ as one, and $P_m$ as 0.05, the proposed algorithm converged at ~30 iteration numbers and achieved optimal solutions. Different runs of the algorithm generate stable results (differences in the results are about 2%) as long as training samples are kept consistent.

## III. Experiment and Analysis

The Zhangjiang estuary in southeastern China, a national mangrove reserve, was chosen as the region for algorithm

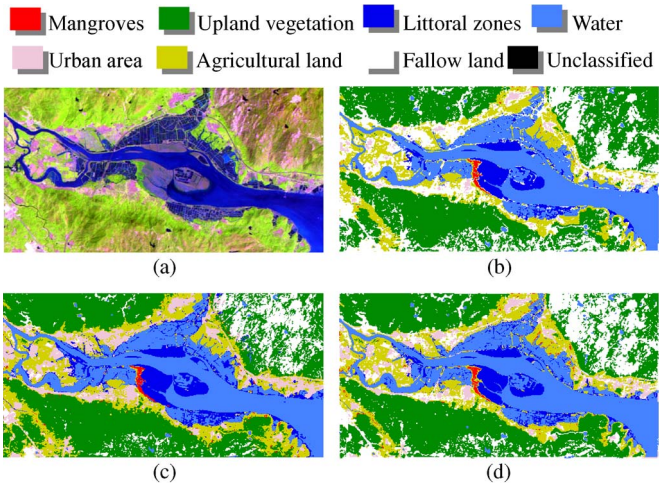


Fig. 2. (a) TM RGB (bands 5, 4, and 3) remote sensing image in the Zhangjiang estuary of southeastern China on September 25, 2006. Classified images derived from (b) AIA, (c) SVM, and (d) ML.

experiment. The reserve is bounded by 22°53′45″ N–23°56′00″ N and 117°24′07″ E–117°30′00″ E, with an area of 2360 ha. A multispectral Landsat TM image (National Aeronautics and Space Administration Landsat Program, 2006, Landsat TM5 scene LT51200432006268BKT00, U.S. Geological Survey, Sioux Falls, September 25, 2006) was used in the experiment [Fig. 2(a)]. Image preprocessing was performed using ENVI 4.5, including atmospheric correction, image enhancement, and geometric rectification, which were established by registering it to a Google Earth image acquired on February 9, 2005, through ground control points. This Google image was also used in the subsequent tasks described as follows.

### A. Decision-Making Features and Land Cover Classification

Spectral, topographic, and textural features are integrated as the decision-making features, since they are proved to be efficient for the classification of remote sensing images [15], [16]. Twelve features, including the spectra of the TM image (band 1–band 7), the digital elevation model (DEM), the normalized difference vegetation index (NDVI), and three textural features of NDVI, were extracted for each sample and stacked into a multidimensional vector that was input into the AIA.

The DEM was obtained from the Advanced Spaceborne Thermal Emission and Reflection Radiometer (ASTER) sensor onboard the Terra satellite with 30-m resolution. Based on an integrated visual interpretation of the Google Earth, the TM, and the ASTER DEM images, we found that the mangrove grew in the areas with the ASTER DEM values of $< 8$ m. We then chose 8 m as a threshold to distinguish the areas with high probability of mangrove growth from the mountain areas with dense vegetation. The pixels with DEM values greater than eight were assigned to real numbers between [0, 0.5], while those of DEM values lesser than 8 m were assigned to real numbers between [0.5, 1].

The NDVI was calculated using ENVI 4.5 with the input of TM spectral data at bands 3 and 4 [17]. The gray-level co-occurrence matrix (GLCM) [18] of NDVI was generated using the same software, with a moving window of $3 \times 3$. Numbers at four directions (0, 45, 90, and 135) were averaged. Three textural variables—variance, dissimilarity, and second moment—were extracted from the GLCM as decision-making features, according to the fact that the texture of mangroves is fine and smooth, whereas other green vegetation is coarse and rippled. Note that, without the textural features involved, the classification results are less satisfied, and the spectral separability of the training class spectra computed using ENVI also demonstrates that the DEM, NDVI, and GLCM features improve separability. Improvement of the accuracies owing to the inclusion of image texture information had also been found for the Maximum Likelihood Classification and neural network techniques [19].

TABLE I
LAND COVER TYPES IN CLASSIFICATION

| Class Name | Land-cover Class | Description |
|---|---|---|
| C1 | Mangroves | Mangrove forests |
| *C2* | Agricultural land | Crop fields, paddy fields and grasslands |
| *C3* | Upland vegetation | Deciduous or evergreen forest land, orchards, and tree groves |
| *C4* | Water | Permanent open water, lakes reservoirs, bays, and estuaries |
| *C5* | Urban area | Residential, commercial, industrial and other developed land |
| C6 | Littoral zones | Land in the intertidal zone or the transitional zone between land and sea |
| C7 | Fallow land | Fields no longer under cultivation |

The training samples were selected by an effort which integrated visual interpretation of the Google Earth image and TM image with field investigation. The number of training samples for each class is 100. Briefly, prior to the fieldwork, candidate samples were identified in the laboratory based on the visual interpretation of the Google Earth image and TM image. On August 27, 2010, a field survey was conducted in the Zhangjiang estuary to validate the sample candidates using a global position system. Seven land cover types and 100 training samples for each type were then determined (Table I).

### B. Experimental Results

In order to assess any improvement in classification accuracy with the AIA, we compared the results with those classified with maximum likelihood (ML) and SVM. The ML and SVM were performed using ENVI 4.5, while the AIA was programmed with MATLAB. The classified images are shown in Fig. 2(b)–(d).

As shown in Fig. 2, all three methods result in good classification for the water and littoral zones. However, for the left five land cover types, ML had serious misclassification and leakage points; many samples of agricultural land and upland vegetation were wrongly identified as mangroves in ML and SVM. The AIA seems to avoid these problems.

### C. Classification Assessment

Two hundred test samples were randomly selected from a WorldView-2 image (1.8-m resolution) and the Google Earth image which had been used for geometric rectification. Overall

TABLE II
COMPARISON OF THE OVERALL ACCURACY

| | AIA | SVM | ML |
|---|---|---|---|
| Overall | 90.2% | 82.6% | 81.6% |
| Kappa | 0.886 | 0.797 | 0.785 |

TABLE III
COMPARISON OF COMMISSION AND OMISSION, AS A PERCENTAGE

| | AIA | | SVM | | ML | |
|---|---|---|---|---|---|---|
| Class | Com | Omi | Com | Omi | Com | Omi |
| C1 | 9.77 | 21.5 | 4.19 | 20.0 | 40.9 | 23.5 |
| C2 | 19.1 | 11.0 | 35.3 | 10.0 | 37.1 | 61.0 |
| C3 | 1.98 | 1.00 | 6.1 | 0.5 | 0.63 | 21.5 |
| C4 | 1.01 | 1.50 | 0.0 | 13.5 | 6.90 | 5.50 |
| C5 | 4.14 | 16.1 | 40.2 | 27.0 | 10.1 | 7.00 |
| C6 | 1.48 | 0.00 | 12.3 | 0.0 | 6.54 | 0.00 |
| C7 | 24.5 | 3.00 | 0.0 | 51.0 | 23.8 | 10.5 |

accuracy and kappa coefficient and the commission and omission of the classifications were then computed.

As shown in Table II, the overall classification accuracy of AIA is 90.2%, and the kappa coefficient is 0.88, both higher than those of ML and SVM. This indicates that the newly developed algorithm can improve the overall classification accuracy effectively. The accuracy of this modified AIA was similar to those derived from other adaptive methods. Using SVM, Huang *et al.* report classification accuracies greater than 90% for red, black, and white mangrove canopies [6]. A novel approach that combined a decision tree with the SVM showed an overall accuracy greater than 94% $(\text{kappa} = 0.863)$ for classifying true mangrove species and other dense coastal vegetation at the object level [8].

The commission and omission of the classifications are shown in Table III. The commission number refers to the percentage of misclassification, while the omission number represents the percentage of unclassification. Table III demonstrates that, in general, low commission and omission numbers are obtained by the AIA. Although the SVM has lower omission and commission errors than AIA for mangroves, it has some very high error numbers for other classes within the framework of this case study.

All of these results demonstrate that the modified AIA developed in this study is a competent classification method for satellite images and is capable of providing an accurate mapping of mangroves. This is not surprising since AIA is a self-adaptive method which is data-driven and can adjust itself to the data without explicit specification of the functional or distributional form of the underlying model.

To characterize further the robustness of the AIA scheme in mangrove mapping, more evaluation experiments with images of higher spectral and spatial resolutions are planned. On the other hand, new satellite sensors have been rapidly developed [20]. Combining radar imagery with optical imagery can potentially improve recognition accuracy further.

## ACKNOWLEDGMENT

The authors would like to thank the two anonymous reviewers for their constructive comments on this letter.

## REFERENCES

[1] D. M. Alongi, "Present state and future of the world's mangrove forests," *Environ. Conserv.*, vol. 29, no. 3, pp. 331–349, 2002.
[2] B. W. Heumann, "Satellite remote sensing of mangrove forests: Recent advances and future opportunities," *Progr. Phys. Geography*, vol. 35, no. 1, pp. 87–108, Feb. 2011.
[3] C. Giri, E. Ochieng, L. Tieszen, Z. Zhu, A. Singh, T. Loveland, J. Masek, and N. Duke, "Status and distribution of mangrove forests of the world using Earth observation satellite data," *Global Ecol. Biogeography*, vol. 20, no. 1, pp. 154–159, Jan. 2011.
[4] L. Wang, W. P. Sousa, P. Gong, and G. S. Biging, "Comparison of IKONOS and QuickBird images for mapping mangrove species on the Caribbean coast of Panama," *Remote Sens. Environ.*, vol. 91, no. 3/4, pp. 432–440, Jun. 2004.
[5] S. Tadjudin and D. A. Landgrebe, "Covariance estimation with limited training samples," *IEEE Trans. Geosci. Remote Sens.*, vol. 37, no. 4, pp. 2113–2118, Jul. 1999.
[6] X. Huang, L. Zhang, and L. Wang, "Evaluation of morphological texture features for mangrove forest mapping and species discrimination using multispectral IKONOS imagery," *IEEE Geosci. Remote Sens. Lett.*, vol. 6, no. 3, pp. 393–397, Jul. 2009.
[7] G. Conchedda, L. Durieux, and P. Mayaux, "An object-based method for mapping and change analysis in mangrove ecosystems," *ISPRS J. Photogramm. Remote Sens.*, vol. 63, no. 5, pp. 578–589, Sep. 2008.
[8] B. W. Heumann, "An object-based classification of mangroves using a hybrid decision tree—Support vector machine approach," *Remote Sens.*, vol. 3, no. 11, pp. 2440–2460, Nov. 2011.
[9] B. Babayigit, K. Guney, and A. Akdagli, "A clonal selection algorithm for array pattern nulling by controlling the positions of selected elements," *Progr. Electromagn. Res.*, vol. 6, pp. 257–266, 2008.
[10] L. N. De Castro and F. J. Von Zuben, "Learning and optimization using the clonal selection principle," *IEEE Trans. Evol. Comput.*, vol. 6, no. 3, pp. 239–251, Jun. 2002.
[11] W. Dong, G. Shi, and L. Zhang, "Immune memory clonal selection algorithms for designing stack filters," *Neurocomputing*, vol. 70, no. 4–6, pp. 777–784, Jan. 2007.
[12] L. Zhang, Y. Zhong, B. Huang, J. Gong, and P. Li, "Dimensionality reduction based on clonal selection for hyperspectral imagery," *IEEE Trans. Geosci. Remote Sens.*, vol. 45, no. 12, pp. 4172–4186, Dec. 2007.
[13] L. N. De Castro and F. J. Von Zuben, "The clonal selection algorithm with engineering applications," in *GECCO—Workshop Proc.*, 2000, pp. 36–39.
[14] R. De Maesschalck, D. Jouan-Rimbaud, and D. Massart, "The Mahalanobis distance," *Chemometrics Intell. Lab. Syst.*, vol. 50, no. 1, pp. 1–18, Jan. 2000.
[15] D. R. Peddle and S. E. Franklin, "Image texture processing and data integration for surface pattern discrimination," *Photogramm. Eng. Remote Sens.*, vol. 57, no. 4, pp. 413–420, Apr. 1991.
[16] K. Liu, X. Li, X. Shi, and S. Wang, "Monitoring mangrove forest changes using remote sensing and GIS data with decision-tree learning," *Wetlands*, vol. 28, no. 2, pp. 336–346, Jun. 2008.
[17] C. J. Tucker, "Red and photographic infrared linear combinations for monitoring vegetation," *Remote Sens. Environ.*, vol. 8, no. 2, pp. 127–150, May 1979.
[18] R. M. Haralick, K. Shanmugam, and I. H. Dinstein, "Textural features for image classification," *IEEE Trans. Syst., Man, Cybern.*, vol. SMC-3, no. 6, pp. 610–621, Nov. 1973.
[19] L. Wang, J. L. Silván-Cárdenas, and W. P. Sousa, "Neural network classification of mangrove species from multi-seasonal Ikonos imagery," *Photogramm. Eng. Remote Sens.*, vol. 74, no. 7, pp. 921–927, Jul. 2008.
[20] M. Wooster, "Remote sensing: Sensors and systems," *Progr. Phys. Geography*, vol. 31, no. 1, pp. 95–100, Feb. 2007.